A Bootstrap Approach for Analyzing the Statistical Properties of SPECT and PET Images

Irene Buvat and Cyril Riddell

Abstract-- **We describe a non-parametric bootstrap method to estimate the statistical properties of Single Photon Emission Computed Tomography (SPECT) and Positron Emission Tomography (PET) images, whatever the type of noise in the projections and the reconstruction algorithm. Using analytical simulations and real PET data, this method is shown to accurately predict the statistical distribution, hence the variance, of reconstructed pixel values for both linear and non-linear reconstruction algorithms.**

I. Introduction

A general method for characterizing the noise properties of Single Photon Emission Computed Tomography (SPECT) and Positron Emission Tomography (PET) images would be useful to study the effect of factors like the injected dose, the reconstruction algorithm or various corrections (scatter, attenuation, random). Noise estimates in reconstructed images could also be introduced into quantitative data analysis to account for the uncertainty of region of interest (ROI) values or when using algorithmic observers for evaluation purposes. For images reconstructed with filtered backprojection (FBP), analytical derivations have been proposed to predict the variance of pixel or ROI values (e.g., [1,2]). For non-linear reconstruction algorithms such as Maximum Likelihood Expectation Maximization (MLEM) and block-iterative reconstruction algorithms, approximations are required to analytically deduce the statistical properties of the reconstructed images from those of the projections [3, 4]. For FBP as well as for iterative reconstruction, all approaches assume Poisson noise in the projections and "noise" sources introduced by processing steps (e.g., scatter correction, interpolation) are ignored or dealt with using simplifying assumptions in the error propagation analysis. A bootstrap approach has already been suggested to investigate the statistical properties of PET images but it also assumed that the recorded counts were Poisson distributed [5].

In this study, we propose a non-parametric bootstrap method to characterize the statistical properties of SPECT or PET images, for any linear or non-linear reconstruction method and whatever the type of noise in the projections.

I. Buvat is with the U494 INSERM, CHU Pitie-Salpetriere, Paris, France (telephone: 33-1-53 82 84 15, e-mail: buvat@imed.jussieu.fr).

C. Riddell is with GE Medical System, Buc, France (e-mail: Cyril.Riddell@med.ge.com).

II. Theory

A. The bootstrap approach

The bootstrap approach is a computer-based statistical method for determining the accuracy of a statistic θ (e.g., median) estimated from experimental data [6]. It requires an experimental sample $x=(x_1, \ldots, x_N)$ whose empirical distribution estimates an unknown distribution F. In this sample, each measurement x_i is considered as a random realization of the variable that follows distribution F. Under its simplest form, the bootstrap uses what is called a plug-in principle:

- Given the empirical sample $x=(x_1, \ldots, x_N)$, draw B independent bootstrap samples $x^b*=(x_1^b*, \ldots, x_N^b*)$ of N elements. Each element x_i^b* is obtained by sampling with replacement from the original empirical sample x.
- For each bootstrap sample x^b*, calculate the statistic of interest $\theta(x^b*)$, which is called a bootstrap replication of θ.
- The set of bootstrap replications $\{\theta(x^b*)\}_{b=1,B}$ yields the bootstrap distribution of θ, from which the statistical behavior of θ can be inferred. For instance, the bootstrap variance M_2 (moment of order 2) of θ is:

$$M_2 = [\ \Sigma_{b=1,B}\ (\theta(\mathbf{x}^b*) - M_1)^2 / (B-1)] \qquad (1)$$

where $M_1 = \Sigma_{b=1,B}\ \theta(\mathbf{x}^b*)/B$ is the mean of θ over the B bootstrap replications.

B. Using the bootstrap concept to get bootstrap sub-sinograms and bootstrap sinograms

When characterizing the statistical properties of a specific SPECT or PET image, the statistic of interest θ is the reconstructed image itself or a parameter derived from it. Using the bootstrap approach therefore requires obtaining B bootstrap reconstructed images $\theta(\mathbf{x}^b*)$ resulting from B bootstrap sinograms $\mathbf{x}^b*$. A sample of empirical sinograms is needed to generate bootstrap sinograms. Such a sample can be obtained by collecting the data in a gated fashion, to distribute the C counts detected during the whole acquisition over N gates so that N statistically independent realizations of sinograms of about C/N counts - called sub-sinograms in the following as they include N times less counts than the total number of acquired counts - are obtained. Alternatively, the data can be acquired in list-mode and reformatted into N statistically independent sub-sinograms. The sub-sinograms provide a small sample that contains some empirical information regarding the statistical distribution of the sub-

0-7803-7324-3/02/$17.00 © 2002 IEEE

sinograms that will be taken advantage of in the non-parametric bootstrap approach.

Each empirical sub-sinogram of about C/N counts is an (A,K) matrix, where A and K are the numbers of projection angles and acquisition bins. A bootstrap sub-sinogram is generated by randomly drawing each row j (corresponding to a specific angle) among the N realizations of row j given by the N empirical sub-sinograms. Rows j and j' of a bootstrap sub-sinogram can thus come from different empirical sub-sinograms. Drawing rows as a whole instead of pixel values is a key step to properly account for the noise correlation potentially present within a row. On the other hand, as noise is not correlated from one row to another, row i can be drawn independently of row j. Using this method, any number B of bootstrap sub-sinograms can be randomly generated among the N^A possible combinations.

Given these B bootstrap sub-sinograms of about C/N counts, B/N bootstrap sinograms of about C counts can be obtained by summing the bootstrap sub-sinograms N by N.

C. Deriving the statistical properties of reconstructed SPECT and PET images

Bootstrap sub-sinograms can be readily used to derive the statistical properties of the corresponding sub-images ("sub-" meaning that they include only about C/N counts) using the plug-in principle [6]. Each of the B bootstrap sub-sinogram is first reconstructed independently. The resulting B sub-images can be used to derive any information regarding the statistical properties of the sub-image reconstructed from a sub-sinogram. For instance, the moment of order k $M_k(i)$ in pixel i is:

$$M_k(i) = [\ \Sigma_{b=1,B}\ (\theta(\mathbf{x}^{b*})_i - \underline{\theta}^*_i)^k\ /\ (B-1)\ ], \qquad (2)$$

where $\theta(\mathbf{x}^{b*})_i$ is the value of pixel i in the sub-image reconstructed from the bootstrap sub-sinogram b* and $\underline{\theta}^*_i$ is the mean value of pixel i over the B reconstructed sub-images.

To estimate the statistical properties of the image reconstructed from the total acquisition of C counts, B/N bootstrap images of about C counts are first reconstructed from the B/N bootstrap sinograms of about C counts obtained by summing the bootstrap sub-sinograms N by N. Using these B/N reconstructed bootstrap images, the moment of different orders can be estimated using Eq. 2, in which the average is calculated over the B/N reconstructed images only. $M_2(i)$ for instance gives the pixel-by-pixel variance of the reconstructed pixel values.

The proposed bootstrap approach used for estimating the statistical properties of reconstructed SPECT and PET sub-images does not include any assumption about the statistical properties of the projections or the error propagation during reconstruction. It should thus be valid whatever the statistical properties of the projections and the reconstruction algorithm.

When applying the bootstrap approach to the images (as opposed to the sub-images), the only underlying assumption is that a sinogram of C counts is identical to a sum of N sinograms of C/N counts that would be acquired in the same conditions. This implies that the on-line corrections (like random correction in PET) that might be applied to the detected events have to be additive (e.g., the number of randoms subtracted from a C count acquisition should be identical to the sum of the number of randoms subtracted from each of the N acquisitions of C/N counts).

III. Material and method

The proposed bootstrap approach was validated by studying whether it accurately predicted the statistical properties of sub-images and images. Numerical simulations for which the statistical properties of the noise could be fully controlled and PET data including empirical noise were used and different reconstruction schemes were considered.

A. Numerical simulations

A SPECT acquisition (128 parallel projections over 360°, 128 bins per projection) of a 2D elliptical object with 3 elliptical regions of uniform activity were simulated using the RECLBL library. The activity ratios in the three inner ellipses with respect to the background were 0:1, 2:1 and 4:1 respectively. Attenuation, scatter and detector response function were not simulated. The noise-free 128×128 sinogram included 77911 counts, with an average value (±1 standard deviation) in non-zero pixels of 5.6±2.9. Thirty noisy realizations of the sinograms were simulated using Poisson noise. Thirty noisy realizations of the sinograms were also obtained using Gaussian noise with a constant variance over all pixels equal to 8.

B. Real PET data

A cardiac phantom (Data Spectrum, Chapel Hill, NC) was considered, with FDG activity in the left ventricle (LV) wall (99.9 MBq/ml), no activity in the LV cavity and in the lungs, and background activity in the rest of the phantom representing the soft tissues (13.32 Mq/ml). A 15 min static PET acquisition of the phantom was performed on a GE-Advance machine operating in 2D mode. The data were acquired as a 40 image gated sequence, using a pulse generator with a 1 second period. The resulting images thus represented 40 statistically independent replicates of a 22.5 second acquisition. The sinograms were corrected for dead time and random. A 32 minute long transmission scan of the phantom was also acquired after the emission scan to get the attenuation coefficient factors that were used to correct the sinograms for attenuation before reconstruction. For this study, the sinogram (281 acquisition bins and 336 projection directions) corresponding to a single slice through the cardiac compartment of the phantom was considered, without and with attenuation correction, yielding 2 data sets presenting different noise properties, as attenuation correction alters the noise properties. Without attenuation correction, the total number of counts in the sinograms was around 144500 with an average pixel value around 2.5±1.8. After attenuation correction, the average pixel value was around 25±21.

C. Statistical properties of the reconstructed sub-images

To check that the statistical properties of the sub-images were accurately predicted using the bootstrap approach, a gold

standard was obtained by simulating 1000 noisy realizations of the numerical phantom affected by Poisson noise and Gaussian noise. For each type of noise, the 1000 noisy sub-sinograms were reconstructed using 3 reconstruction schemes: filtered backprojection with a Ramp filter (cut-off frequency of 0.5 pixel^{-1}) (FBP-Ramp), FBP with a Hann filter (cut-off frequency of 0.3 pixel^{-1}) (FBP-Hann), and Ordered Subset Expectation Maximization with 8 subsets and 3 iterations (OSEM24). For each type of noise in the sinograms and each reconstruction scheme, the statistical distribution of reconstructed pixel values were characterized from these 1000 reconstructed sub-images using: 1) the histograms of reconstructed pixel values; 2) the moment of order 2 (variance); 3) the moment of order 3 divided by $M_2(i)^{3/2}$ which corresponds to the skewness coefficients characterizing the departure of the statistical distribution from zero.

These figures of merit were compared to the corresponding figures of merit calculated using the bootstrap approach. For each type of noise, 30 noisy sub-sinograms were used to generate 1000 bootstrap sub-sinograms. These were reconstructed using the 3 schemes previously mentioned and the statistical distribution of the resulting bootstrap sub-images were characterized using the figures of merit.

For the PET cardiac data without and with attenuation correction, the 40 empirical replicates were reconstructed using the 3 reconstruction schemes. The 40 resulting sub-images were used to get a rough estimate of the statistical properties of the reconstructed sub-images, providing an imperfect "gold standard". These statistical properties were compared to those estimated using the bootstrap approach: for each of the two data sets (without and with attenuation correction), 1000 bootstrap sinograms were calculated from the 40 sub-sinograms and reconstructed. The statistical properties of the resulting sub-images were then characterized.

D. Statistical properties of the images

Validation of the accurate prediction of the statistical properties of images was performed using numerical simulations only, as only in that case could a gold standard be easily obtained. For Poisson or Gaussian noise, 1000 noisy realizations of a sinogram including 30 times more counts than the sub-sinograms were performed. These noisy realizations were reconstructed using the 3 reconstruction schemes and the statistical properties of the resulting images were characterized using the moments corresponding to the variance and the skewness. On the other hand, 30000 bootstrap sub-sinograms were calculated from the 30 noisy sub-sinograms and then grouped 30 by 30 to yield 1000 bootstrap sinograms. These 1000 bootstrap sinograms were reconstructed using the 3 reconstruction schemes and the statistical properties of the reconstructed images were derived.

IV. Results and Discussion

A. Statistical properties of reconstructed sub-images

Simulations. For the numerical simulation with Poisson noise reconstructed with FBP-Ramp, Fig. 1 shows an example of the histogram of reconstructed pixel values obtained using the 1000 noisy sub-sinograms that were simulated (gold standard) and using the 1000 bootstrap sub-sinograms calculated from 30 noisy sub-sinograms only. There was an excellent agreement between the two histograms, demonstrating that the bootstrap approach accurately predicted the full statistical distribution of reconstructed pixel values using only 30 noisy sub-sinograms. The same observation held for Gaussian noise and for the 3 reconstruction schemes (results not shown).

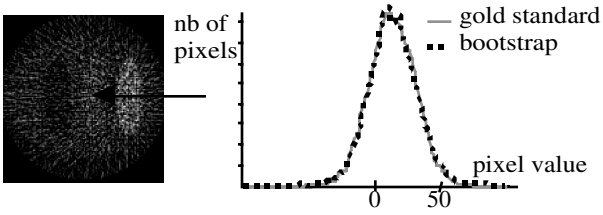

Fig. 1. FBP-RAMP reconstructed sub-image for the Poisson simulation and histogram of pixel values in the region shown by an arrow: the distribution of pixel values as estimated using the bootstrap from 30 noisy replicates (dotted line) agreed well with the distribution of pixel values obtained using 1000 noisy replicates (plain gray line).

Table I gives the average percent differences in pixel standard deviation (σ) estimated using the bootstrap approach and using the 1000 noisy simulations (gold standard):

$100\times$ (estimated σ – gold standard σ)/gold standard σ.

This average difference was calculated over the pixels inside the outer ellipse.

TABLE I
AVERAGE PERCENT DIFFERENCES IN STANDARD DEVIATION VALUES ASSOCIATED WITH RECONSTRUCTED SUB-IMAGE PIXEL VALUES (± 1 STANDARD DEVIATION) BETWEEN THE BOOTSTRAP ESTIMATES AND THE GOLD STANDARD FOR THE NUMERICAL SIMULATIONS

Reconstruction scheme	Poisson noise	Gaussian noise
FPB-Ramp	-1.3±3.4	-1.4±3.4
FBP-Hann	-1.3±3.4	-1.9±3.3
OSEM24	-1.3±9.5	-1.7±11.4

This table shows that the standard deviation value associated with each pixel value was accurately estimated using the bootstrap approach for the two types of noise and for the 3 reconstruction schemes. The higher variability of the percent difference observed for OSEM24 sub-images compared to FBP sub-images (standard deviation around 9 instead of 3 for Poisson noise) results from the fact that when sub-images are reconstructed with OSEM, the standard deviation in each pixel is strongly correlated with the reconstructed pixel value, thus low standard deviation values are observed in pixels with low values [3]. For instance, for the Poisson simulated data reconstructed with FBP-RAMP, the standard deviation values were about 13 for pixels with reconstructed values around 1 and were about 18 for pixels with reconstructed pixel values around 27, while for OSEM24, the standard deviations were about 1 and 8.5 respectively for pixels with reconstructed values around 1 and 27 respectively. Therefore, with OSEM24, for those pixels with very low standard deviation in the "gold standard σ image", a small error in the standard deviation estimate

caused a high percent difference in standard deviation values, hence the higher variability of the percent difference between estimated and gold standard σ observed for OSEM24.

Real PET data. For the real PET data with sub-sinograms corrected for attenuation and reconstructed using OSEM24, Fig. 2a shows the standard deviation image associated with the reconstructed sub-images as estimated using the 40 empirical replicates and using the bootstrap approach. Profiles across these images (Fig. 2b) show that the bootstrap estimate is a low noise estimate of that obtained when using only the 40 empirical replicates.

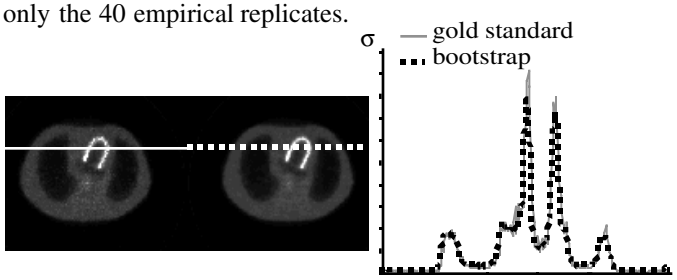

a: gold standard bootstrap b: horizontal profiles

Fig. 2. a. Standard deviation images associated with the PET phantom sub-images reconstructed using OSEM24 as estimated using the 40 empirical replicates (left) and the bootstrap approach (right). b. profiles through the standard deviation images.

The average differences in pixel standard deviation estimated from the 40 empirical replicates and from the bootstrap approach are summarized in Table II for the 3 reconstruction schemes and for the sub-sinograms corrected for attenuation or not.

TABLE II
AVERAGE PERCENT DIFFERENCES IN STANDARD DEVIATION VALUES ASSOCIATED WITH THE RECONCTRUCTED SUB-IMAGE PIXEL VALUES (± 1 STANDARD DEVIATION) BETWEEN THE EMPIRICAL AND THE BOOTSTRAP ESTIMATES FOR THE PET PHANTOM

Reconstruction scheme	Without AC	With AC
FPB-Ramp	1.9±12.1	1.9±12.0
FBP-Hann	1.8±12.1	1.9±12.1
OSEM24	1.9±18.0	5.1±19.4

Table II shows that for real noise as observed in experimental PET data, which is no more Poisson or Gaussian but most probably spatially correlated due to the corrections applied on the data (dead time, random and optionally attenuation), the bootstrap approach yielded an accurate estimate of the standard deviation value associated with each reconstructed pixel value. The variability of the percent differences between estimated and "gold standard" standard deviation values was higher for the PET data (Table II) than for the numerical simulations (Table I). The reason is that for the PET data, the "gold standard" was imperfect since it was derived from 40 experimental measurements only, hence it was more noisy than the gold standard as calculated for the numerical simulations by simulating 1000 noisy realizations of the sinograms.

Increased accuracy in standard deviation estimates resulting from the bootstrap approach. The experiments performed using the simulations and the PET data demonstrate that when a small number of realizations of a specific configuration are available (30 for the simulations and 40 for the PET data in our examples), using the bootstrap makes it possible to predict the statistical properties of reconstructed sub-images with a high accuracy. Table III illustrates the gain in accuracy resulting from the use of the bootstrap (B=500) as a function of the number of available empirical samples for the Poisson simulation reconstructed using FBP-RAMP and OSEM-24. For a given number of empirical samples, using the bootstrap reduces the bias with which the standard deviations associated with reconstructed pixel values are estimated and reduces the variability of this bias by a factor between 2 and 5. Using 30 empirical replicates and the bootstrap yields an estimate of pixel-by-pixel standard deviations as good as and even better than (in terms of variability of the bias) that obtained using 100 empirical replicates without the bootstrap. For simulations and phantom experiments, the bootstrap is thus as a useful adjunct to increase the power of the statistical tests that might be performed using the reconstructed images, by yielding accurate estimates of the standard deviations associated with reconstructed pixel values.

TABLE III
AVERAGE PERCENT ERRORS IN STANDARD DEVIATION ESTIMATES ASSOCIATED WITH THE RECONSTRUCTED SUB-IMAGE PIXEL VALUES (± 1 STANDARD DEVIATION) DEPENDING ON THE NUMBER OF SUB-SINOGRAMS AVAILABLE AND ON WHETHER THE BOOTSTRAP XAS USED

Nb of samples and processing scheme	FBP-RAMP	OSEM24
5 without bootstrap	-15.4±30.8	-20.2±39.0
5 with bootstrap	-10.3±5.3	-11.7±19.1
10 without bootstrap	-7.9±22.0	-10.8±31.0
10 with bootstrap	-5.2±4.5	-6.1±15.1
30 without bootstrap	-2.0±12.8	-3.3±19.7
30 with bootstrap	-1.3±3.4	-1.3±9.5
100 without bootstrap	-0.5±6.7	-0.8±11.1

B. Statistical properties of reconstructed images

Simulations. For the numerical Poisson simulation reconstructed using FBP-Hann, Fig. 3 shows the images of pixel standard deviations estimated using the 1000 noisy realizations of the sinograms and using the bootstrap performed from the 30 noisy realizations of sub-sinograms. The profiles drawn across the images confirm that the bootstrap accurately estimated the standard deviation associated with reconstructed pixel values.

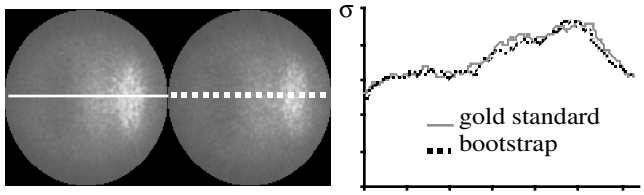

a: gold standard bootstrap b: horizontal profiles

Fig. 3. a: Standard deviation images associated with the image reconstructed using FBP-Hann from the Poisson numerical simulation as estimated using 1000 noisy replicates (gold standard, left) and using the bootstrap approach from 30 noisy replicates of sub-sinograms (right). b: profiles through the standard deviation images.

Table IV lists the average differences in pixel standard deviation σ estimated using the bootstrap approach and using the 1000 noisy replicates of the sinogram, for the 3 reconstruction schemes and for the two types of noise. This table demonstrates that the bootstrap approach using 30 noisy sub-sinograms obtained by splitting the total acquisition in 30 accurately predicted the standard deviations associated with the pixel values reconstructed from the total acquisition.

TABLE IV
AVERAGE PERCENT DIFFERENCES IN STANDARD DEVIATION VALUES ASSOCIATED WITH THE RECONSTRUCTED IMAGE PIXEL VALUES (± 1 STANDARD DEVIATION) BETWEEN THE BOOTSTRAP ESTIMATES AND THE GOLD STANDARD FOR THE NUMERICAL SIMULATIONS

Reconstruction scheme	Poisson noise	Gaussian noise
FPB-Ramp	-1.2±3.4	-1.5±3.5
FBP-Hann	-1.3±3.3	-2.0±3.4
OSEM24	-1.2±9.4	-2.6±12.5

Figure 4 shows the pixel-by-pixel skewness coefficients obtained using the noisy replicates and using the bootstrap approach for the Poisson simulation reconstructed using FBP-RAMP and OSEM24. The bootstrap approach properly showed that for FBP-RAMP, the statistical distribution of the reconstructed pixel values was symmetrical in all pixels, while it was skewed in low count pixels with OSEM24. The asymmetrical statistical distributions of reconstructed pixel values in the low count regions observed with OSEM24 are a consequence of the non-negativity constraint included in the OSEM algorithms.

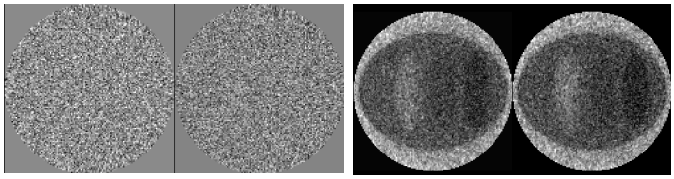

a. FBP-RAMP gold standard | bootstrap | b. OSEM24 gold standard | bootstrap

Fig. 4. Images of the skewness coefficients as estimated from the noisy replicates (gold standard) and from the bootstrap for the Poisson simulation reconstructed using FBP-RAMP (a) and OSEM24 (b).

C. Impact of the number of empirical sub-sinograms for estimating image statistical distribution

To estimate the statistical distribution of a reconstructed image, the bootstrap approach requires the acquired data to be split into N sub-sinograms (section II B). For a fixed total number of counts, the best number of sub-sinograms to be considered has to be studied, as the larger the number of sub-sinograms, the smaller the number of counts in each. Using the Poisson simulations and 500 bootstrap realizations, we found that the average differences in pixel standard deviation (± 1 standard deviation) estimates using the bootstrap approach and the 1000 noisy replicates of the sinogram (gold standard) were -10.0±5.1, -4.8±4.5, -2.4±4.2, -1.2±3.4 and -1.1±4.1 for N = 5, 10, 20, 30 and 40 respectively for FBP-RAMP. The corresponding values were -9.6±9.2, -4.9±9.5, -3.1±9.4, -1.2±9.4 and -1.3±9.5 for OSEM24. This suggests that the larger the number of sub-sinograms that can be acquired or simulated, the smaller the bias affecting the standard deviation estimates. This is consistent with the fact that low count sinograms including more noise best describe the noise properties of the acquired data.

D. Impact of the number of bootstrap realizations

When studying the statistical properties of reconstructed images, the number B of bootstrap realizations to be generated from the N sub-sinograms available must be appropriately chosen. Using the Poisson simulations and N=30 sub-sinograms, we found that the averaged differences in pixel standard deviation estimates derived from the bootstrap approach and from the 1000 noisy replicates of the sinogram (gold standard) were -3.4±12.0, -1.9±7.4, -1.5±5.6, -1.4±4.0 and -1.3±3.4 for B = 30, 100, 200, 500 and 1000 respectively for FBP-RAMP. The corresponding values were -4.5±21.6, -2.1±14.5, -1.7±12.0, -1.4±10.1 and -1.3±9.5 for OSEM24. Using at least B=200 bootstrap realizations thus already yields an accurate estimate of the standard deviation distributions associated with pixel values. The precise number to be considered should then be chosen as a function of the computational burden associated with the reconstruction of B bootstrap sinograms.

V. CONCLUSION

We introduced and validated a bootstrap approach to estimate the statistical distribution of PET and SPECT reconstructed images whatever the noise properties in the projections and the reconstruction algorithm. The approach can be used when several empirical replicates of the same configurations are available: it then greatly increases the accuracy and reduces the variability with which the statistical properties of the reconstructed images can be estimated. It can also be used when a single acquisition is available, for instance in clinical studies, to derive the standard deviation associated with the measurements performed on the reconstructed volume.

VI. ACKNOWLEDGMENT

The authors are grateful to Stephen Bacharach, from the National Institutes of Health in Bethesda, for providing the gated PET data.

VII. REFERENCES

[1] N.M. Alpert, W.C. Barker, A. Gelman, S. Weise, M. Senda, and J.A. Correia, "Estimation of the local statistical noise in emission computed tomography," *IEEE Trans. Med. Imaging*, vol. 1, pp. 142-146, 1982.

[2] R.E. Carson, Y. Yan, M.E. Whiterspoon, N. Freedman, and S.L. Bacharach, "An approximation formula for the variance of PET region-of-interest values," *IEEE. Trans. Med. Imaging*, vol. 12, pp. 240-250, 1993.

[3] H.H. Barrett and B.M.W. Tsui, "Noise properties of the EM algorithm: I. Theory," *Phys. Med. Biol.* vol 39, pp. 833-846, 1994.

[4] E.J. Soares, C.L. Byrne and S.J. Glick. "Noise characterization of block-iterative reconstruction algorithms: I. Theory," *IEEE Trans. Med. Imaging*, vol. 19, pp. 261-270, 2000.

[5] D.R. Haynor and S.D. Woods. "Resampling estimates of precision in emission tomography," *IEEE Trans. Med. Imaging*, vol. 8, pp. 337-343, 1989.

[6] B. Efron and R.J. Tibshirani. *An introduction to the bootstrap.* New York, London. Chapman & Hall, 1993.